JCI insight

RESEARCH ARTICLE

Essential role of IFN-γ in T cell–associated intestinal inflammation

Yoshihiro Eriguchi,[1] Kiminori Nakamura,[2] Yuki Yokoi,[2] Rina Sugimoto,[2] Shuichiro Takahashi,[3] Daigo Hashimoto,[3] Takanori Teshima,[3] Tokiyoshi Ayabe,[2] Michael E. Selsted,[1] and André J. Ouellette[1]

[1]Department of Pathology and Laboratory Medicine, Norris Comprehensive Cancer Center, Keck School of Medicine, University of Southern California, Los Angeles, California, USA. [2]Department of Cell Biological Science, Graduate School of Life Science, Faculty of Advanced Life Science, Hokkaido University, Sapporo, Japan. [3]Department of Hematology, Hokkaido University Faculty of Medicine, Sapporo, Japan.

Paneth cells contribute to small intestinal homeostasis by secreting antimicrobial peptides and constituting the intestinal stem cell (ISC) niche. Certain T cell–mediated enteropathies are characterized by extensive Paneth cell depletion coincident with mucosal destruction and dysbiosis. In this study, mechanisms of intestinal crypt injury have been investigated by characterizing responses of mouse intestinal organoids (enteroids) in coculture with mouse T lymphocytes. Activated T cells induced enteroid damage, reduced Paneth cell and Lgr5$^+$ ISC mRNA levels, and induced Paneth cell death through a caspase-3/7–dependent mechanism. IFN-γ mediated these effects, because IFN-γ receptor–null enteroids were unaffected by activated T cells. In mice, administration of IFN-γ induced enteropathy with crypt hyperplasia, villus shortening, Paneth cell depletion, and modified ISC marker expression. IFN-γ exacerbated radiation enteritis, which was ameliorated by treatment with a selective JAK1/2 inhibitor. Thus, IFN-γ induced Paneth cell death and impaired regeneration of small intestinal epithelium in vivo, suggesting that IFN-γ may be a useful target for treating defective mucosal regeneration in enteric inflammation.

Introduction

Paneth cells of the small intestinal epithelium contribute to small bowel homeostasis (1). First, they secrete α-defensins (2), which both confer immunity to *Salmonella enterica* serovar Typhimurium infection (3) and select the composition of the ileal microbiota (4–6). Also, they contribute to crypt stability by releasing niche signals for maintenance of Lgr5$^+$ crypt intestinal stem cells (ISCs), which position themselves to optimize surface contact with Paneth cells (7), and Paneth cells stimulate ISC numbers to expand during caloric restriction via mTORC1 signaling (8). Thus, physiologic events that impair Paneth cell health and viability jeopardize enteric homeostasis, representing risk factors associated with inflammatory bowel diseases.

Paneth cell homeostasis is sensitive to proinflammatory conditions that induce Paneth cell depletion and may impair the ability of crypt ISCs to proliferate and regenerate the epithelial barrier. For example, loss of Paneth cells is associated with the onset of inflammation in graft-versus-host disease (GVHD) (9–11), during *Toxoplasma gondii* infection (12, 13), and in autoimmune enteropathy (AIE) (14–17). The subsequent reductions in mucosal defense mechanisms and the resulting dysbiosis exacerbate inflammation and may compromise tissue repair by disturbing the ISC crypt microenvironment. In GVHD, loss of Paneth cells is associated with gut dysbiosis and bacterial translocation across the epithelial barrier (9, 10), which positively correlates with mortality (9–11). Similarly, in mice infected with *T. gondii*, activated CD4$^+$ Th1 cells and intestinal dysbiosis both induce transient, IFN-γ–dependent elimination of Paneth cells (12, 13). Immune responses to the parasite are complex, in that germ-free mice do not develop intestinal pathology during *T. gondii* infection (12). The microbiota activated Paneth cell–specific autophagy via induction of IFN-γ, and deletion of Atg5 in Paneth cells exacerbated intestinal immunopathology in response to *T. gondii* infection (13).

In ex vivo studies investigating Paneth cell degranulation, IFN-γ was identified as mediating release of host defense molecules into the lumen of cultured enteroids (18). Enteroids, small intestinal crypt organoids, consist of a 3D epithelial monolayer that maintains crypt-villus architecture with replicating ISCs that differentiate into the major small intestinal epithelial lineages (19). Exposure of enteroids to IFN-γ induced

Conflict of interest: The authors have declared that no conflict of interest exists.

Submitted: April 26, 2018
Accepted: August 14, 2018
Published: September 20, 2018

Reference information:
JCI Insight. 2018;3(18):e121886.
https://doi.org/10.1172/jci.insight.121886.

Paneth cells to extrude their secretory granules and nuclei. Also, IFN-γ increased the number of enteroid cells positive for cleaved caspase-3, although FACS analyses did not identify which cells were positive for activated caspase (18). In addition, exposure of enteroids to IFN-γ reduced Paneth cell and ISC marker expression, and induced MHC class II expression in all enteroid cells (18), suggesting that IFN-γ exerts direct adverse effects on all intestinal epithelial populations.

To improve understanding of effector mechanisms that mediate crypt injury by activated T cells, we investigated mouse enteroids in coculture with activated T cells to identify mediators of inflammation-induced Paneth cell loss. Using this ex vivo system, we identified proinflammatory mediators released by activated T cells and characterized enteroid responses to specific cytokines, demonstrating that IFN-γ targets Paneth cells and Lgr5$^+$ ISCs. Subsequently, we showed that systemic administration of IFN-γ to mice disturbed ileal crypt homeostasis in vivo, and crypts depleted of Paneth cells by IFN-γ were highly sensitive to injury by sublethal irradiation and failed to recover.

Results

Activated T cells induce enteroid damage associated with Paneth cell and Lgr5$^+$ ISC loss ex vivo. Because activated donor T cells are primarily responsible for GVHD etiology (9, 10), and parasite-induced Th1 cells are associated with Paneth cell elimination (12), we tested whether activated T cells secrete factors that disrupt the intestinal epithelium. Studying mouse enteroids cultured ex vivo allowed epithelial responses to T cell activation to be isolated from possible humoral or paracrine factors released by gut stromal cells, distal tissues, or the gut microbiota. Activation of mouse splenic CD4$^+$ or CD8$^+$ T cells with anti-CD3/28 in coculture with enteroids (Figure 1, A and B) induced enteroid damage within 2 days, with increasing severity over 3–4 days (Figure 1, B–E); but in the absence of T cells, anti-CD3/28 had no effect on enteroid integrity (data not shown). The lack of damage in cocultures with resting T cells demonstrated the requirement for T cell activation (Figure 1, B, D, and E).

Because the number of recognizable Paneth cells is reduced in GVHD (9) and *T. gondii* infection (12), lineage-specific marker mRNAs in enteroids incubated with activated or resting T cells were quantified to test for selective reductions in Paneth cells and Lgr5$^+$ ISCs. Quantitative reverse transcription PCR (qRT-PCR) analyses showed that levels of Paneth cell α-defensin-22 (*Defa22*) and ISC *Lgr5* mRNAs were reduced in enteroids incubated for 1–2 days with activated but not resting T cells (Figure 2, A–D). Enteroids embedded in Matrigel did not contact T cells directly (Figure 1B), suggesting that soluble factors released by activated T cells affected Paneth cell and ISC marker mRNA expression. Exposure to activated CD8$^+$ T cells caused a greater reduction in Paneth cell and ISC marker mRNA levels than did CD4$^+$ T cells, implying that CD8$^+$ T cells release higher levels of, or additional, enteroid-damaging factors.

IFN-γ induces enteroid damage and Paneth cell and Lgr5$^+$ ISC loss. To identify T cell mediators of enteroid damage, ELISAs were performed to measure cytokines in mixed culture media from 1 to 4 days after T cell activation. Levels of IFN-γ, TNF-α, IL-2, and IL-17A secreted by activated CD4$^+$ and CD8$^+$ T cells increased relative to unactivated T cells (Supplemental Figure 1, A–J; supplemental material available online with this article; https://doi.org/10.1172/jci.insight.121886DS1). Only low levels of IL-6 secretion were detected, and none of the cytokines were released by unactivated T cells. Accordingly, enteroids exposed to secreted cytokines at the highest levels detected (Supplemental Figure 1, A–J) were evaluated for loss of integrity. At 2 ng/ml, IFN-γ damaged enteroids within 2 days, but no other cytokine tested affected enteroid integrity (Figure 3, A and B). The effects of IFN-γ on enteroid epithelial lineages were tested by quantifying lineage marker mRNAs, including *Defa22* (Paneth cells), *Lgr5* (rapidly cycling ISCs), *Bmi1* (quiescent ISCs), *Muc2* (goblet cells), *Dclk1* (tuft cells), *Chga* (enteroendocrine cells), and *Alpi* (enterocytes) in enteroids treated with IFN-γ for 3 days. Relative to control enteroids not exposed to cytokines, IFN-γ reduced *Defa22* mRNA 450-fold and *Lgr5* mRNA 24-fold (Figure 3C), but effects of IFN-γ on *Dclk1*, *Muc2*, and *Chga* mRNAs were modest, and *Bmi1* and *Alpi* mRNA levels were not affected significantly (Figure 3C). All lineage marker mRNAs remained at normal levels in enteroids exposed to all other cytokines tested (Figure 3C).

IFN-γ induces dose-dependent loss of Paneth cells and rapidly cycling ISCs. To assess the relative contribution of activated CD4$^+$ and CD8$^+$ T cell–derived IFN-γ to the induction of Paneth cell and Lgr5$^+$ ISC loss, enteroids were cultured for 3 days with IFN-γ at levels released by both activated T cell populations. At 500 pg/ml, the maximum level of IFN-γ released by CD4$^+$ T cells (Supplemental Figure 1A), enteroid damage was extensive (Figure 4), and mRNA levels for Paneth cell markers Defa22, Defa5, pan-cryptdins, and lysozyme were reduced significantly by IFN-γ in a dose-dependent manner (Figure 5A and Supplemental Figure 2, A–C).

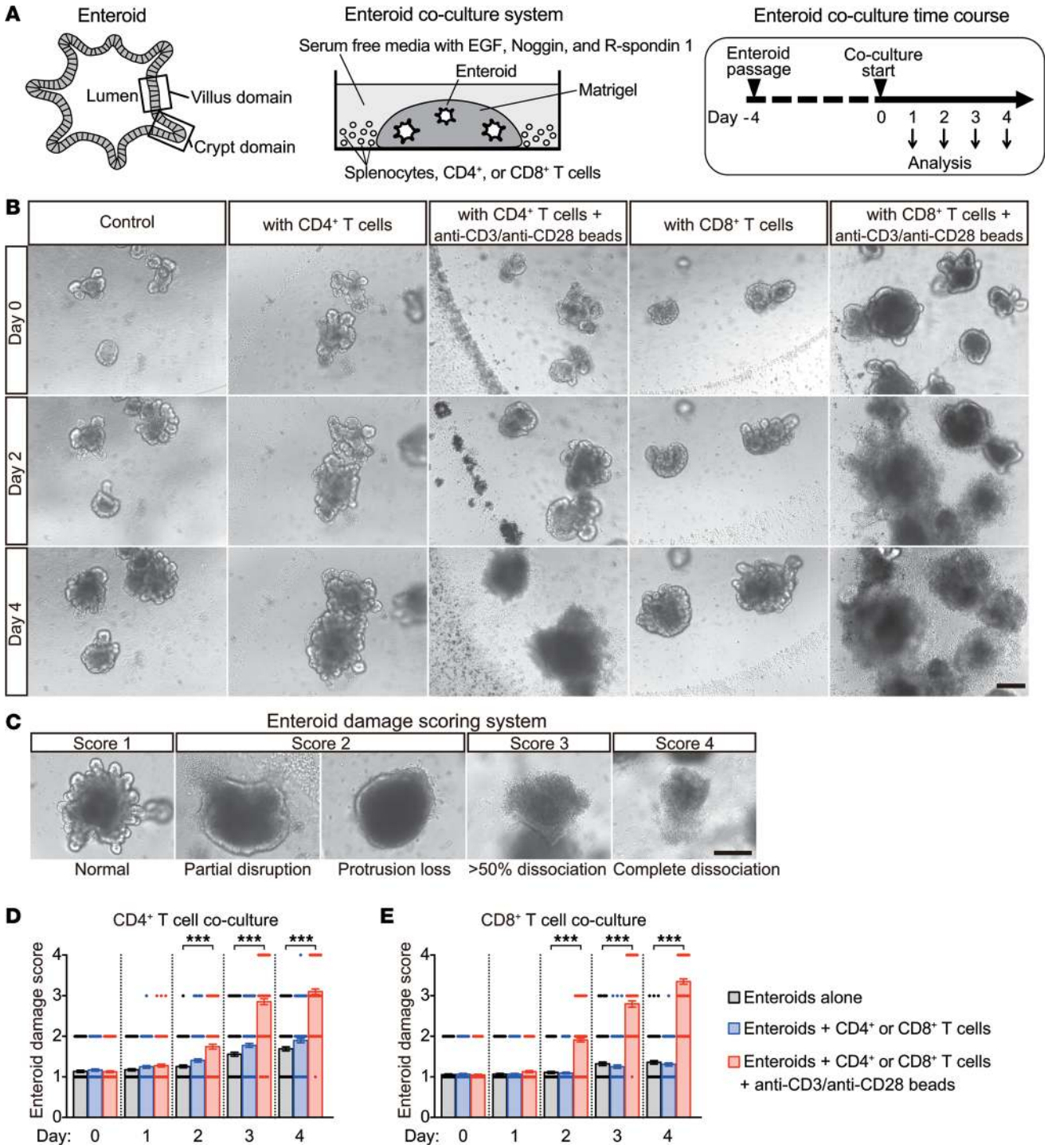

Figure 1. Activated T cells induce enteroid damage. (**A**) Overall design of enteroid and T cell coculture experiments. (**B**) Enteroids cocultured with CD4$^+$ or CD8$^+$ T cells (5×10^4 cells per well) with (activated) or without (resting) anti-CD3/anti-CD28 beads. (**C**) Enteroid damage scoring system. Damage scores of enteroids cocultured with CD4$^+$ (**D**) or CD8$^+$ (**E**) T cells. Data are representative of 2 independent experiments and are shown as mean ± SEM (n = 100 enteroids per group); gray bars, enteroids alone; blue bars, enteroids plus resting T cells; red bars, enteroids plus activated T cells. Dunnett's multiple comparisons test was used to compare each group with the control group. ***$P < 0.001$. Scale bars: 200 μm.

Also, levels of *Lgr5* and *Olfm4* mRNAs, markers of rapidly cycling ISCs downstream of Wnt and Notch signaling (20, 21), decreased (Figure 5, C and D), as did mRNAs for Paneth cell niche factors *Wnt3* and Notch ligand *Dll4* (Figure 5, E and F). *Bmi1* mRNA levels were similar to controls (Figure 5B), as were mRNAs that mark the other major epithelial lineages (Supplemental Figure 2, D–G). We conclude that the quantity

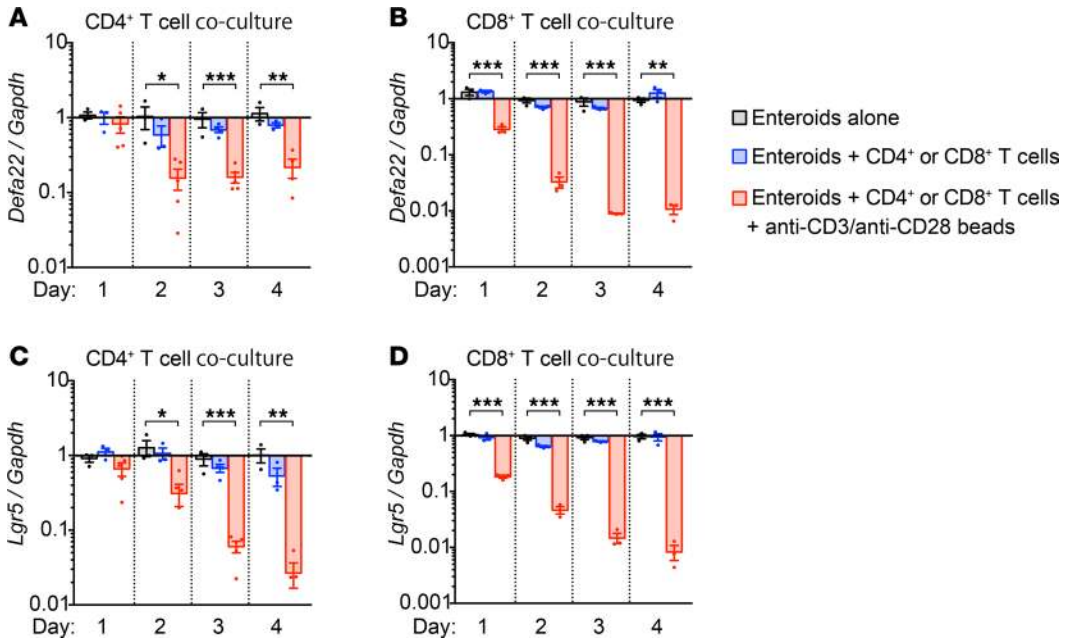

Figure 2. Activated T cells reduce Paneth cell and Lgr5$^+$ ISC marker mRNA levels. (**A**–**D**) Enteroids cocultured with CD4$^+$ or CD8$^+$ T cells (5×10^4 cells per well) with (activated) or without (resting) anti-CD3/anti-CD28 beads. After removal of CD4$^+$ (**A** and **C**) and CD8$^+$ (**B** and **D**) T cells, enteroid RNAs were analyzed by qRT-PCR to measure levels of *Defa22* (**A** and **B**) and *Lgr5* (**C** and **D**) mRNAs. Data are representative of 2 independent experiments and shown as mean ± SEM (enteroids alone, $n = 3$ independent wells, gray bars; enteroids + resting T cells, $n = 4$, blue bars; enteroids + activated T cells, $n = 4$, red bars). Dunnett's multiple comparisons test was used to compare each group with the control group. $^*P < 0.05$, $^{**}P < 0.01$, $^{***}P < 0.001$.

of IFN-γ secreted by CD4$^+$ T cells is sufficient to induce loss of enteroid integrity, but CD8$^+$ cell activation is judged to have a greater impact on enteroid Paneth cells and Lgr5$^+$ ISCs, because they release 4 times more IFN-γ than CD4$^+$ T cells.

IFN-γ induces Paneth cell death through a caspase-3/7–dependent pathway. In a previous study, the overall fraction of enteroid cells positive for cleaved caspase-3 increased with IFN-γ exposure, although the identities of the positive cells were not reported (18). To identify enteroid cells that have apoptotic responses to IFN-γ exposure (18), we tested whether IFN-γ specifically induces Paneth cell death by quantifying *Casp3* mRNA. Over 3 days, IFN-γ increased enteroid *Casp3* mRNA dose-dependently (Figure 5G), and its sustained expression contrasted with the reduced levels of Paneth cell marker mRNAs (Figure 5A), suggesting that IFN-γ was inducing *Casp3*-dependent Paneth cell death. To test for cleaved caspase-3 in Paneth cells, caspase-3/7 activity was visualized by live confocal microscopy of enteroids exposed to 2 ng/ml IFN-γ (Figure 6 and Supplemental Videos 1 and 2), which showed that caspase-3/7 activation occurred in Paneth cells within 13–16 hours of cytokine exposure (Figure 6 and Supplemental Videos 1 and 2). Concurrent with caspase-3/7 activation, Paneth cells extruded their cell contents into the crypt lumen, as previously reported (18). We conclude that reduction of Paneth cell marker mRNAs by IFN-γ occurs by selective induction of cell death by caspase-3/7 activation.

IFN-γ is required for induction of enteroid damage by activated splenocytes. To test whether Paneth cell and ISC depletion depended exclusively on IFN-γ, we measured IFN-γ receptor–null (IFN-γRKO) enteroid responses to coculture with activated splenic T cells. As before (Figure 1B), activated splenocytes from C57BL/6 (WT) mice induced damage in WT enteroids within 2–4 days, but IFN-γRKO enteroids grew and differentiated normally under the same coculture conditions (Figure 7, A and B). WT enteroids cocultured with activated T cells for 4 days had markedly reduced levels of Paneth cell *Defa22* and ISC *Lgr5* mRNAs. In contrast, *Defa22* mRNA levels remained normal, and *Lgr5* mRNA was only slightly lower in IFN-γRKO enteroids under the same conditions (Figure 7C). Whether the 2- to 4-fold changes in other lineage markers are meaningful relative to the magnitude of effects on WT Paneth cells and Lgr5$^+$ ISCs is unclear (Figure 7C). The moderate reduction in the ISC, enteroendocrine cell, and enterocyte markers in cocultured IFN-γRKO enteroids (Figure 7C) suggests that cytokines other than IFN-γ from activated T cells also may induce damage, but to a lesser extent. Activated

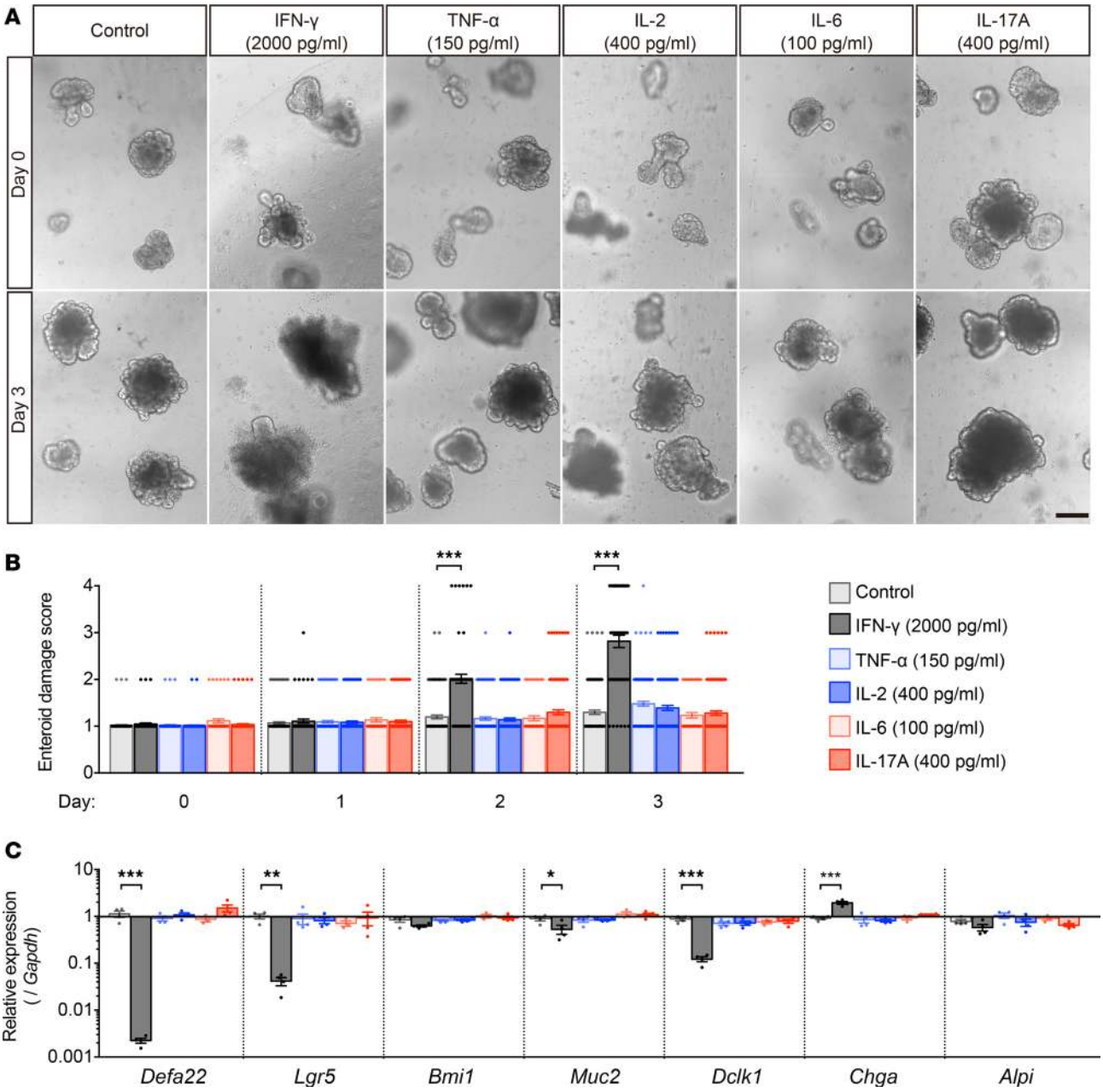

Figure 3. IFN-γ induces enteroid damage. (**A**) Enteroids were exposed to IFN-γ, TNF-α, IL-2, and IL-17A, the highest levels released into coculture media, or with 100 pg/ml in the case of IL-6 to determine which cytokine(s) mediate enteroid damage. Only IFN-γ treatment caused damage. (**B**) Damage scores of enteroids exposed for 3 days to the proinflammatory cytokines shown. Data are from 2 independent experiments and shown as mean ± SEM (n = 100 enteroids per group). (**C**) qRT-PCR analyses of lineage markers in enteroids exposed to cytokines for 3 days. Data are representative of 2 independent experiments and shown as mean ± SEM (n = 4 independent wells). Dunnett's multiple comparisons test was used to compare each group with the control group. *P < 0.05, **P < 0.01, ***P < 0.001. Scale bar: 200 μm.

T cells increased *Casp3* mRNA ~6-fold in WT enteroids but not in IFN-γR knockouts (Figure 7C). We conclude that IFN-γ signaling mediates selective Paneth cell and Lgr5$^+$ ISC depletion under induced proinflammatory conditions.

IFN-γ receptor 1 expression on both Paneth cells and Lgr5$^+$ ISCs. To test for the lineage-specific expression of the IFN-γ receptor, single-cell suspensions of CD24^{hi}Lgr5-EGFP^{lo} Paneth cells and Lgr5-EGFP^{hi} ISCs isolated from *Lgr5-GFP-CreERT2* mouse small intestinal crypts were analyzed via flow cytometry for IFN-γ receptor 1 (Ifngr1) expression (Supplemental Figure 3, A–D). The data show that Paneth cell and Lgr5$^+$ ISC levels of Ifngr1 were equivalent (Supplemental Figure 3, E and F), and a priori both crypt

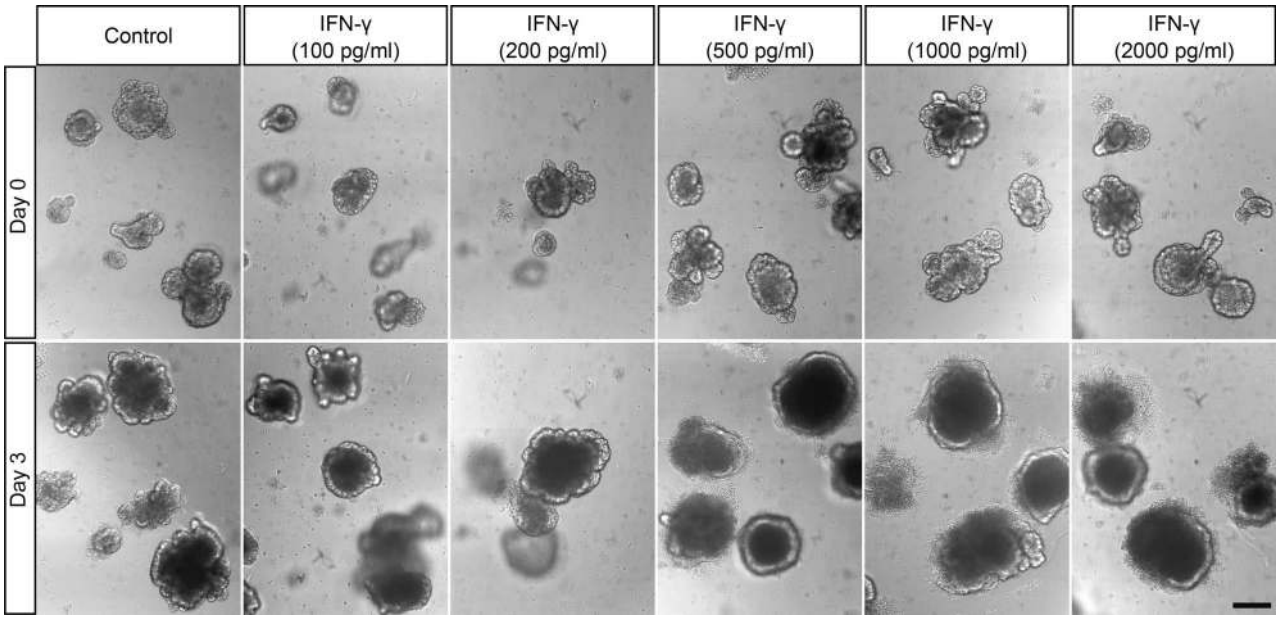

Figure 4. IFN-γ induces dose-dependent enteroid damage. Enteroids were exposed to IFN-γ for 3 days as shown. Representative images from 2 experiments are shown. Scale bar: 200 μm.

subpopulations appear to be equally capable of responding to IFN-γ. Accordingly, determining whether IFN-γ exerts direct or indirect effects on Paneth cells or Lgr5$^+$ ISCs will require analyses of lineage-specific conditional knockouts.

Ruxolitinib prevents IFN-γ–induced enteroid damage. To test whether the effects of IFN-γ could be prevented with targeted therapy, WT enteroids treated with IFN-γ were cultured with 0.1–10 μM ruxolitinib, a selective inhibitor of JAK1/2 in IFN-γ signaling (22). Ruxolitinib inhibited IFN-γ signaling in enteroids, as confirmed by suppression of *Socs1* gene expression (Supplemental Figure 4C), and it diminished IFN-γ–induced enteroid damage dose-dependently without affecting enteroid integrity, growth, or differentiation (Supplemental Figure 4, A and B). Ruxolitinib blocked IFN-γ–induced *Casp3* expression (Supplemental Figure 4D) and prevented reductions in *Defa22*, *Lgr5*, and *Olfm4* mRNAs, which remained at normal levels (Supplemental Figure 4, E, G, and H). Ruxolitinib did not alter enteroid *Bmi1* mRNA levels regardless of IFN-γ challenge (Supplemental Figure 4F). Thus, IFN-γ induces selective effects on Paneth cells and ISCs in enteroids that are prevented by ruxolitinib.

Exogenous IFN-γ depletes Paneth cells and disrupts the ileal crypt niche in mice. IFN-γ released by activated T cells disrupts enteroid integrity and crypt homeostasis by selective reduction of Paneth cells and Lgr5$^+$ ISCs, and T cell activation also induces IFN-γ–dependent Paneth cell loss in vivo (12, 18). The effects of IFN-γ on rapidly cycling ISCs in vivo were tested by i.p. administration to mice, followed by immunofluorescence and histochemical staining of terminal ileal samples (Figure 8A). Paneth cell numbers and levels of the Paneth cell α-defensin Defa1 (cryptdin-1) were reduced in ileum by IFN-γ treatment (Figure 8, C, F, and I, and Figure 9E), and crypts that were positive for Lgr5 and Olfm4 decreased with exogenous IFN-γ administration (Figure 9, F and G). Although IFN-γ reduced Olfm4 staining in ileal crypts (Figure 8I), diffuse Lgr5 immunofluorescence still was detected in crypts that lacked apparent Paneth cells (Figure 8F). These findings suggest that exogenous IFN-γ resulted in replacement of Lgr5$^+$ and Olfm4$^+$ rapidly cycling ISCs with Lgr5^{lo} and Olfm4–negative (Lgr5^{lo}Olfm4$^-$) cells in association with apparent loss of Paneth cells. In vivo IFN-γ treatment reduced ileal *Defa22* mRNA ~300-fold and *Olfm4* mRNA ~30-fold, but *Lgr5* mRNA levels were nearly normal in ileum (Figure 9H), consistent with the immunohistological findings (Figure 8F). Exogenous IFN-γ modified ileal morphology, inducing villus shortening and crypt elongation (Figure 8C and Figure 10B). These defects resemble a phenotype common in GVHD (9), *T. gondii* infection (12), and AIE (14–16, 23), suggesting that IFN-γ contributes to disease pathogenesis. Compared with the ~300-fold reduction in ileal *Defa22* mRNA, IFN-γ treatment had modest effects on other ileal lineage markers (Figure 9H), except for enterocyte *Alpi* mRNA,

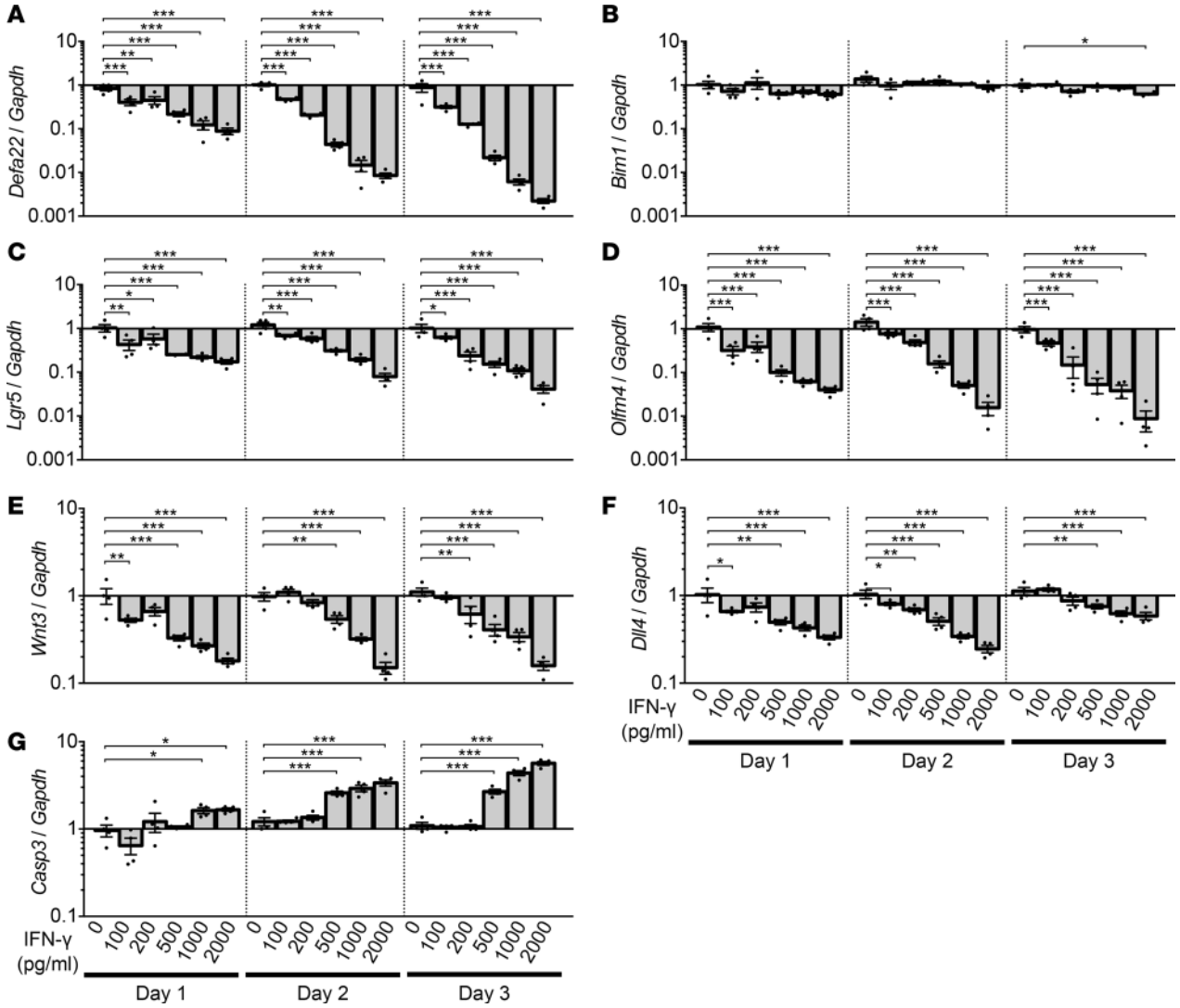

Figure 5. IFN-γ induces dose-dependent loss of Paneth cells and rapidly cycling stem cells. Enteroids were exposed to IFN-γ for 3 days. (**A**–**G**) qRT-PCR analyses to quantify lineage-specific mRNAs, niche signal mRNAs of Paneth cell origin, and apoptosis mRNA levels in enteroids exposed to IFN-γ for 1, 2, and 3 days. Data are from 2 independent experiments and are shown as mean ± SEM (n = 4 independent wells). Dunnett's multiple comparisons test was used to compare each group with the control group at each time point. *$P < 0.05$, **$P < 0.01$, ***$P < 0.001$.

which was reduced as a possible consequence of the shortened ileal villi (Figure 8C). As in enteroids, inhibition of IFN-γ signaling by ruxolitinib in vivo protected Paneth cells and rapidly cycling ISCs in ileum (Figure 8, D, G, and J, and Figure 9, E–H). Thus, exogenous IFN-γ caused ileal Paneth cell depletion, with Lgr5^{lo}Olfm4^{-} cell replacement of Lgr5^{+}Olfm4^{+} ISCs (Figure 8, F and I) and disruption of normal crypt-villus architecture (Figure 8C and Figure 10B). These findings demonstrate that exogenous IFN-γ alters the ileal niche in vivo in a manner resembling enteroid exposure to IFN-γ ex vivo.

IFN-γ increases intestinal radiosensitivity and associated mortality. Because IFN-γ disrupted rapidly cycling ISCs in vivo (Figure 8, C, F, and I), we tested its effects on the regenerative response to radiation injury. Mice that received IFN-γ were subjected to sublethal total body irradiation (TBI), followed by reconstitution with syngeneic bone marrow cells 24 hours after IFN-γ administration (Figure 11A). All TBI mice treated with IFN-γ (TI) developed profuse diarrhea beginning 32 hours after TBI and died within 2 days. In contrast, cohorts treated only with IFN-γ (I), receiving only TBI (T), or TI mice receiving ruxolitinib (TIR) did not develop diarrhea, recovered from body weight loss and clinical manifestations within 7 days of TBI, and all survived (Figure 11, B–D).

To evaluate the combined effects of IFN-γ and irradiation on ileal homeostasis and pathology, we collected full-length intestines from T, TI, and TIR mice 2 days after TBI; from I mice and mice treated

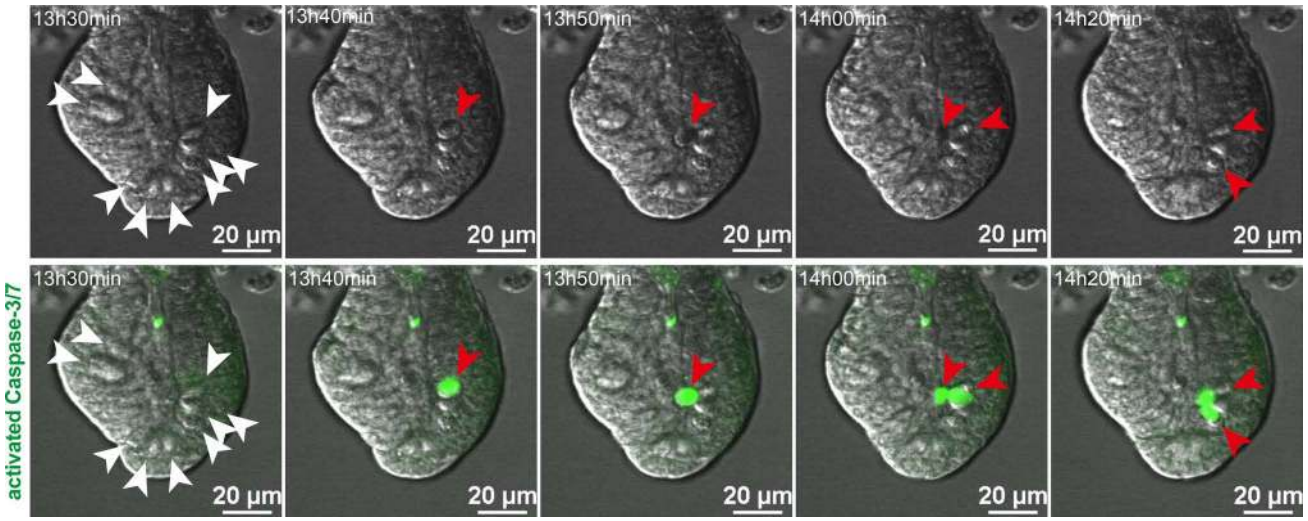

Figure 6. IFN-γ induces Paneth cell death through a caspase-3/7–dependent pathway. Still images from time-lapse analysis of caspase-3/7 activity in an enteroid exposed to IFN-γ (from Supplemental Videos 1 and 2). Paneth cells (white arrowheads) are granule-containing and appear white in the differential interference contrast images (top row). Cells containing activated caspase-3/7 have bright green nuclei (red arrowheads), which were detected only in Paneth cells and extruded into the crypt lumen after caspase-3/7 activation (bottom row). Time after addition of 2 ng/ml IFN-γ is indicated in the upper left corner of each image. Representative images from 2 experiments are shown. Scale bars: 20 μm.

with IFN-γ + ruxolitinib without TBI (IR); and from control cohorts (C), which received only vehicle (Figure 9, A and B). In TI mice, the small intestinal lumen contained watery fluid (Figure 9B), and the intestine had contracted significantly in length compared with all cohorts except I mice (Figure 9, B and C, and Supplemental Tables 2 and 3). The terminal ilea of TI mice were depleted of Paneth cells and had disrupted crypt-villus architecture, with thinning of the epithelial lining (Figure 11F).

TI induced differential effects on expression of ISC markers. For example, TI ileal *Olfm4* mRNA was markedly reduced relative to control ileum, but *Lgr5* mRNA levels were only ~3-fold lower (Figure 9H). The modest effects on *Lgr5* mRNA levels appear to be inconsistent with the severity of crypt-villus destruction and the reduced numbers of $Lgr5^+$ crypts in TI ileum (Figure 9F and Figure 11, F and I). Their weak and diffuse immune staining suggested that $Lgr5^+$ ISCs had been depleted. Also, Olfm4 and Defa1 staining both were diminished (Figure 9, E and G, and Figure 11, I and L), and, as observed in I mice, TI reduced ileal *Defa22* mRNA levels markedly (Figure 9H). To evaluate ileal disruption further, crypts in ileal cross sections were counted, which showed that IFN-γ reduced the number of crypts per circumference to 83% of the number in control ileum, and TI further reduced the number to 65% of control values (Figure 9D and Supplemental Tables 2 and 3). Thus, the loss of Paneth cells and $Lgr5^+Olfm4^+$ ISCs induced by TI appears to impair epithelial regeneration secondary to depletion of functional rapidly cycling ISCs. Consequently, the total number of functioning crypts decreased with concomitant bowel shortening.

Consistent with villus shortening and crypt loss (Figure 11F), TI also reduced enterocyte and goblet cell numbers, as evidenced by the respective ~450-fold and 26-fold decreases in *Alpi* and *Muc2* mRNAs (Figure 9H). Reductions in *Defa22* and Paneth cell niche factor mRNA levels in TI and I cohorts were not significantly different (Figure 9, H and I), showing that the additive effects of irradiation on Paneth cells in IFN-γ–treated mice were modest. Similarly, levels of mRNAs marking other ileal epithelial lineages were not significantly different between the TI and I groups (Figure 9H).

As observed in enteroids (Supplemental Figure 4) and in ileum of IFN-γ–treated mice (Figure 8, D, G, and J, and Figure 9, E–H), ruxolitinib partially prevented the loss of ileal Paneth cells and rapidly cycling ISCs of TI mice, as well as IFN-γ–induced alterations to the crypt niche environment and differentiation factors (Figure 9, E–I, and Figure 11, G, J, and M). Also, ruxolitinib restored the number of crypts per ileum cross section, reduced contraction of the intestine (Figure 9, B–D), and conferred 100% survival on TIR mice (Figure 11B). Thus, ruxolitinib treatment may restore homeostasis from intestinal inflammation secondary to Paneth cell depletion mediated by IFN-γ.

IFN-γ modulation of ileal crypt cell proliferation in response to irradiation injury. To assess the combined effects of IFN-γ and irradiation on the proliferation status of cells in ileal crypts, the number and distribution

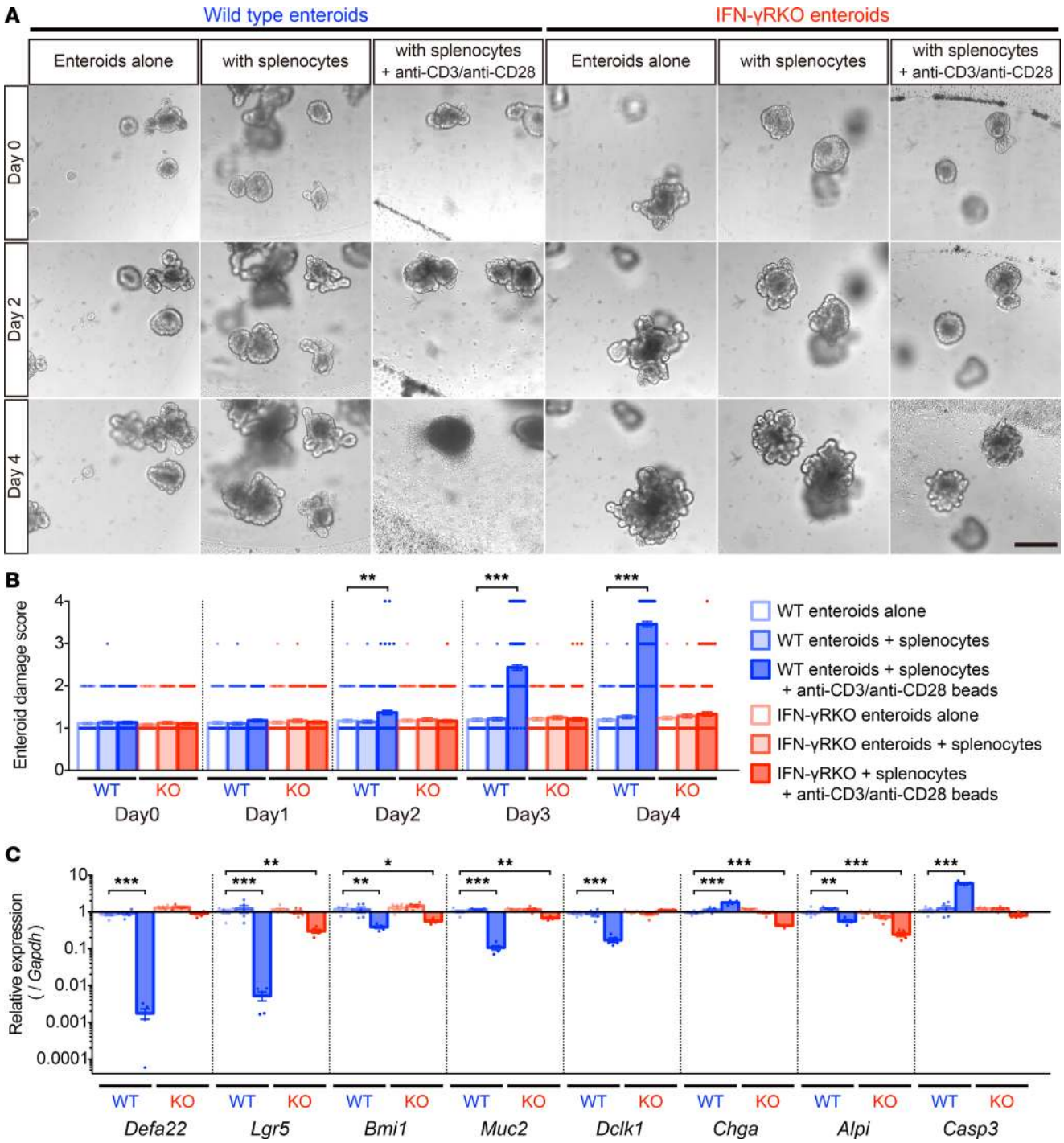

Figure 7. IFN-γ mediates enteroid damage induced by splenocyte activation. (**A**) WT or IFN-γ receptor–KO (IFN-γRKO, KO) enteroids in coculture with WT splenocytes with or without activation using anti-CD3/anti-CD28 beads. (**B**) Damage scores of WT or KO enteroids in coculture with control or activated WT splenocytes. Data are representative of 2 independent experiments and shown as mean ± SEM, with n = 100 enteroids per group. (**C**) qRT-PCR analyses to quantify lineage-specific and apoptosis marker mRNAs in WT or IFN-γRKO enteroids in coculture with control or activated WT splenocytes for 4 days. Data are representative of 2 independent experiments and shown as mean ± SEM (n = 5 independent wells). Dunnett's multiple comparisons test was used to compare each group with the WT control group. *P < 0.05, **P < 0.01, ***P < 0.001. Scale bar: 200 μm.

of Ki-67$^+$ cells were quantified on a per-crypt basis. With IFN-γ administration, the number of crypt Ki-67$^+$ cells increased, and crypt Ki-67$^+$ cells became abundant at the crypt base in place of Ki-67$^-$ Paneth cells and slender Ki-67$^+$ rapidly cycling cells (Figure 10, B and C). In contrast, in irradiated mice, IFN-γ reduced Ki-67$^+$ crypt cell numbers and increased radiosensitivity (Figure 10, B and C). These data are

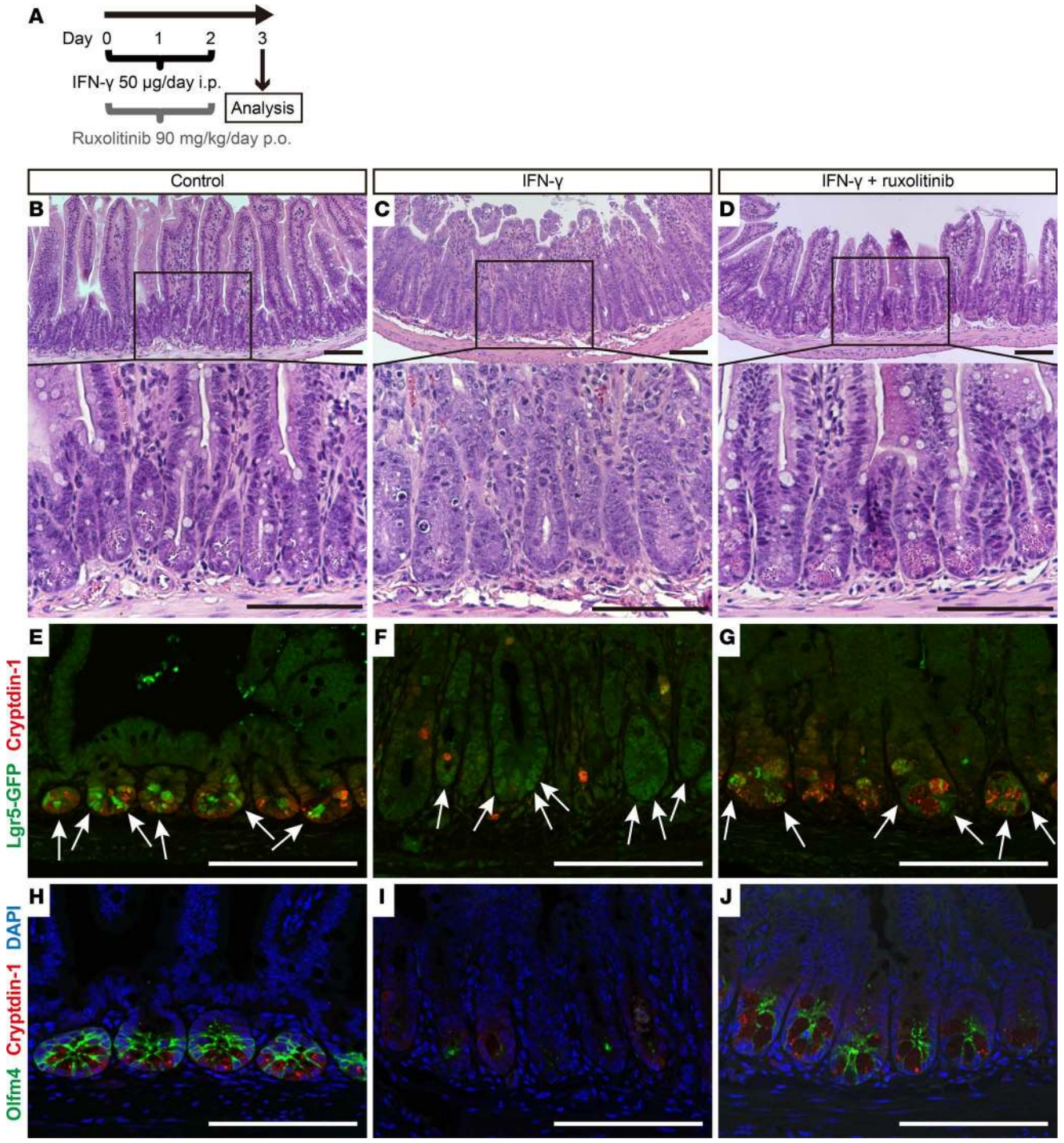

Figure 8. Exogenous IFN-γ depletes Paneth cells and modifies the expression of rapidly cycling ISC markers in vivo. (**A**) Overall experimental scheme for IFN-γ and ruxolitinib administration in mice. Ileum samples were collected 72 hours after the first dose of IFN-γ. Histochemical staining (H&E) of ileum sections from control (**B**), IFN-γ–treated (**C**), or IFN-γ + ruxolitinib–treated (**D**) C57BL/6 mice. (**E**–**J**) Confocal image for cryptdin-1 (red) of *Lgr5-EGFP-ires-creERT2* mouse ileum sections. (**E**–**G**) Lgr5-GFP$^+$ ISCs are green (white arrows). (**H**–**J**) Sections stained for Olfm4 (green) with DAPI (blue). Control (**E** and **H**), IFN-γ–treated (**F** and **I**), and IFN-γ + ruxolitinib–treated (**G** and **J**) ileum sections are shown. The results are representative of 2 experiments. Note that some ileal crypts of IFN-γ–treated mice lack Paneth cells and Olfm4$^+$ ISCs (**I**), but crypts that are faintly positive for Lgr5-GFP cells are still evident (**F**). Scale bars: 100 μm.

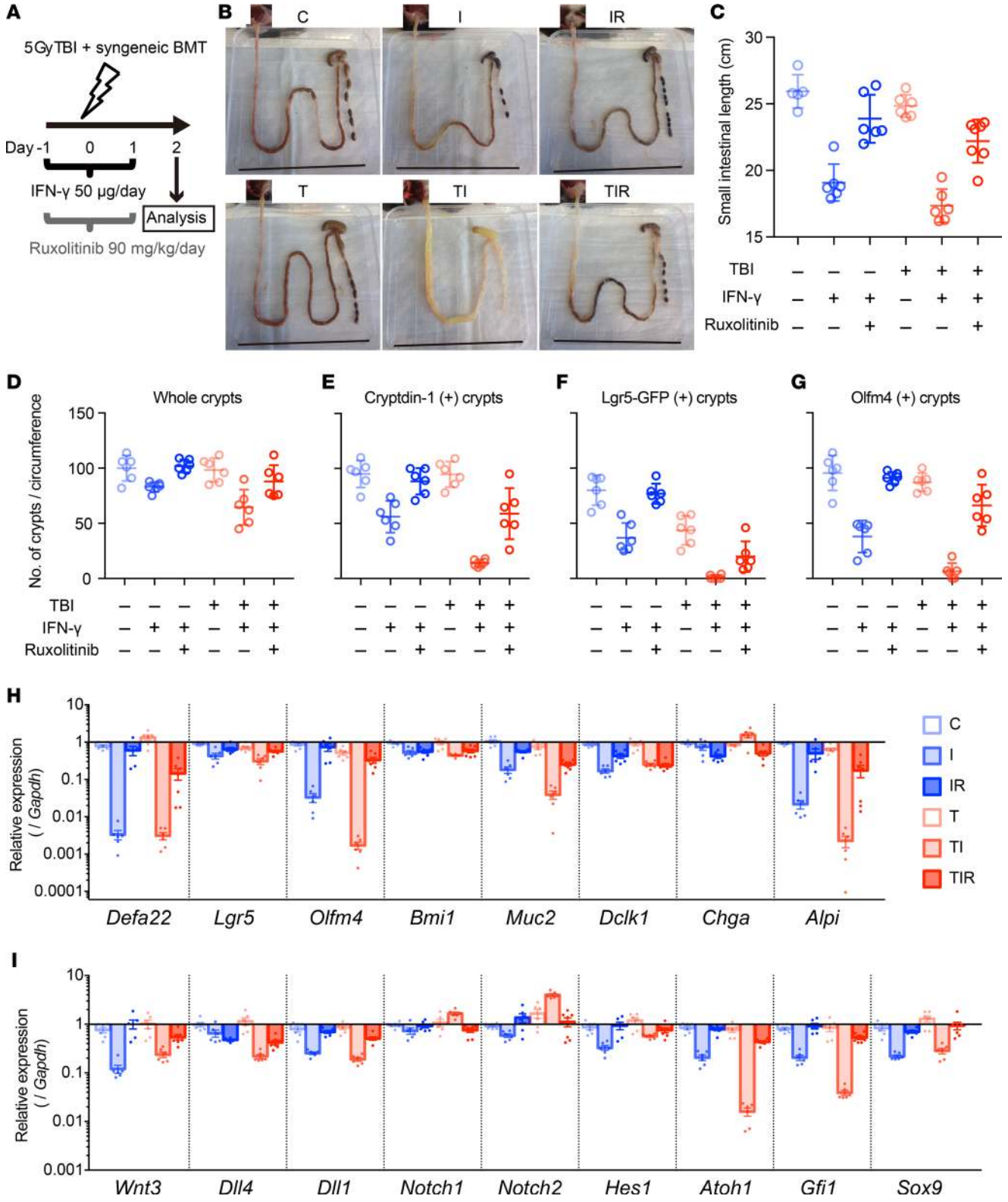

Figure 9. Aggravated radiation enteropathy and impaired epithelial regeneration induced by IFN-γ. (**A**) Schematics of the study to determine effects of TBI, IFN-γ, and ruxolitinib on intestinal epithelium in mice. Ileum tissue was collected 48 hours after TBI and analyzed. (**B**) Representative small intestines of control (C), IFN-γ (I), IFN-γ + ruxolitinib (IR), TBI (T), TBI + IFN-γ (TI), and TBI + IFN-γ + ruxolitinib (TIR) mice are shown. Scale bars: 8 cm. (**C**) Lengths of small bowels in cohort. Measurements from 2 experiments were combined and presented as mean ± SD; control group, $n = 4$; TIR, $n = 7$; remaining groups, $n = 6$. (**D**–**G**) Quantification of crypt numbers per ileum circumference section at 48 hours after TBI. Whole (**D**), cryptdin-1$^+$ (**E**), Lgr5-GFP$^+$ (**F**), and Olfm4$^+$ (**G**) crypts were counted in 2 ileum circumference sections of 3 different *Lgr5-EGFP-ires-creERT2* mice from each group. Data are from 2 separate experiments and show mean ± SD. (**H** and **I**) qRT-PCR analyses were performed to quantify mRNAs coding for

lineage-specific markers, niche factors, and requisite lineage-determining transcription factors in whole terminal ileum tissue. Data from 2 separate experiments were combined and are shown as mean ± SEM; TIR group, $n = 7$; all other groups, $n = 6$ biological replicates. Tukey's multiple comparisons test was used to compare each cohort. Mean values of data in **C–G** and statistical results in **C–I** are presented in Supplemental Tables 2–4.

consistent with disruption of rapidly cycling ISCs in vivo by IFN-γ, although whether IFN-γ effects are mediated directly or indirectly by the Paneth cell niche remains unknown. Ruxolitinib ameliorated the effect of IFN-γ on crypt cell proliferation regardless of irradiation injury (Figure 10, B and C).

Discussion

We have investigated molecular mechanisms by which activated $CD4^+$ and $CD8^+$ T cells mediate small intestinal injury. These studies were prompted, in part, by prior findings that GVHD is mediated by activated donor T cells after allogeneic hematopoietic stem cell transplantation in which Paneth cells are primary targets, and their loss correlates positively with GVHD mortality (9–11). In mouse crypt enteroids cocultured with activated T cells, IFN-γ from activated T cells mediated loss of epithelial enteroid integrity and induced Paneth cell loss via caspase-3/7 activation. In addition, IFN-γRKO enteroids were unresponsive to activated splenic T cells, demonstrating that IFN-γ was the soluble mediator of Paneth cell and rapidly cycling ISC loss. The rescue of enteroid integrity and prevention of Paneth cell death by ruxolitinib further confirmed the role of IFN-γ in targeting the intestinal epithelium. Because Paneth cells and $Lgr5^+$ ISCs both express Ifngr1 (Supplemental Figure 3), whether IFN-γ acted directly or indirectly on Paneth cells and $Lgr5^+$ ISCs remains unknown. Recently, the gut microbiota was shown to activate Paneth cell–specific autophagy by inducing IFN-γ, and the Paneth cell–restricted deficiency in autophagy led to intestinal pathology mediated by TNF-α and IFN-γ (13), providing insight into the basis of Paneth cell sensitivity to IFN-γ.

To test whether enteroid responses to IFN-γ predict its effects in vivo, we administered IFN-γ systemically and determined its consequences on mouse ileum integrity and on recovery of mice from irradiation injury. Consistent with ex vivo findings, i.p. administration of IFN-γ in vivo depleted ileal Paneth cells, impaired recovery, and exacerbated morbidity and mortality in radiation-induced enteritis. IFN-γ greatly reduced expression of the rapidly cycling ISC marker Olfm4 but had only a negligible effect on *Lgr5* expression in ileum (Figure 9H).

In vivo in *Atoh1*-null mice, crypts are Paneth cell deficient but still maintain normal crypt architecture and $Lgr5^+$ ISC function (24, 25). Ex vivo, however, *Atoh1*-null crypts fail to grow and cannot differentiate into enteroids without Wnt supplementation (24). Furthermore, Wnt3 is not required in vivo for maintenance of ISCs in mice, but crypt organoids in culture require Paneth cell–derived Wnt3 in order to develop (20). These findings imply that a Wnt source other than epithelial cells exists in vivo, perhaps deriving from stromal telocytes (26–28). Accordingly, the persistence of Lgr5 expression and its modified distribution pattern in ileum after IFN-γ administration (Figure 8, F and I) may be due to alternative Wnt signals from mesenchymal stromal cells following induced Paneth cell loss. Although IFN-γ–treated mice survived without TBI exposure, IFN-γ administration enhanced sensitivity to sublethal irradiation injury (Figure 11, B–D).

The ileal pathology observed in mice after IFN-γ administration is consistent with reported IFN-γ–induced enteropathy with crypt hyperplasia (29). The results suggest that depletion of Paneth cells removes niche factors that they contribute normally to the crypt environment (30), perhaps inducing conversion of $Lgr5^+$ ISCs to the transit-amplifying (TA) cell compartment, where $Lgr5^+Olfm4^+$ ISCs may differentiate or be replaced by $Lgr5^{lo}Olfm4^-$ cells. IFN-γ administration resulted in loss of $Ki\text{-}67^-$ Paneth cells from the crypt base and replacement with $Ki\text{-}67^+$ rapidly cycling cells and increased numbers of $Ki\text{-}67^+$ cells in crypts, possibly contributing to crypt hyperplasia (Figure 8, C and F, Figure 10, and Figure 12). We speculate that the restructured crypt cell subpopulations may be deficient in responding to irradiation-induced injury (Figure 11), perhaps because quiescent ISCs cannot differentiate into adequate numbers of functional rapidly cycling ISCs and TA cells that were depleted by radiation injury (Figure 10, B and C, and Figure 12). Of potential clinical relevance, patients with chronic inflammation and elevated levels of IFN-γ may have increased risk of enteropathy after abdominal irradiation or systemic chemotherapy.

Our findings suggest that ruxolitinib may be a candidate for treating IFN-γ–induced Paneth cell loss. In the severe and prolonged inflammation of GVHD (9–11) driven by IFN-γ from activated T cells, the clinical outcome is made worse by systemic infections coincident with Paneth cell loss, dysbiosis, and

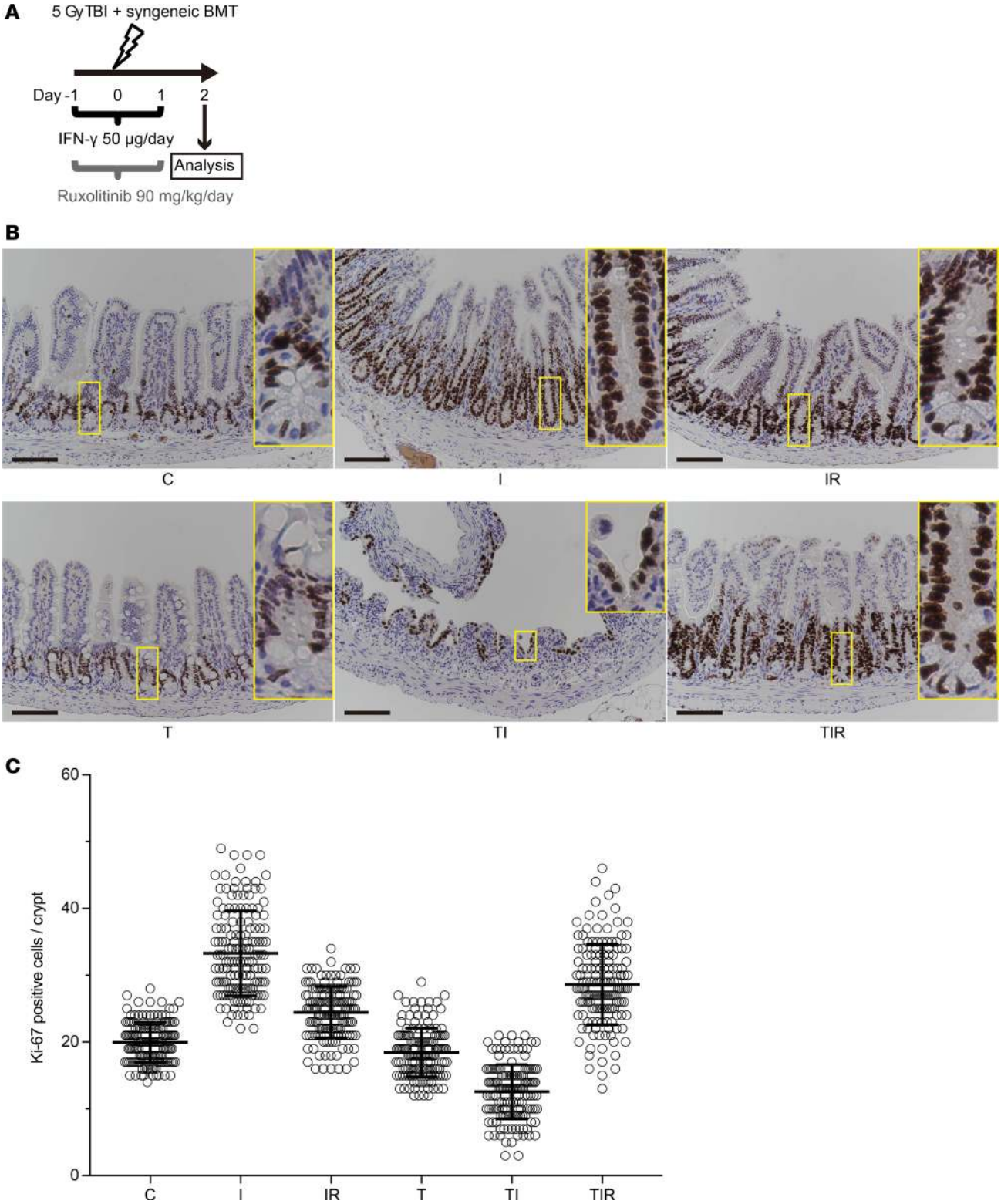

Figure 10. IFN-γ modulation of ileal crypt cell proliferation in response to irradiation injury. (**A**) Schematics of the study to determine effects of TBI, IFN-γ, and ruxolitinib on intestinal epithelium in mice. Ileum tissue was collected 48 hours after TBI and analyzed. (**B**) IHC staining of Ki-67 in mouse ileal sections. Control (C), IFN-γ (I), IFN-γ + ruxolitinib (IR), TBI (T), TBI + IFN-γ (TI), and TBI + IFN-γ + ruxolitinib (TIR) are shown. Scale bars: 100 μm. (**C**) Ki-67$^+$ cell numbers per longitudinal crypt section were counted in 30 ileal crypts per mouse. Data from 5 different C57BL/6 mice in each group were combined from 2 separate experiments and are shown as mean ± SD. Tukey's multiple comparisons test was used to compare the each cohort. Statistical results of data in **C** are presented in Supplemental Table 5.

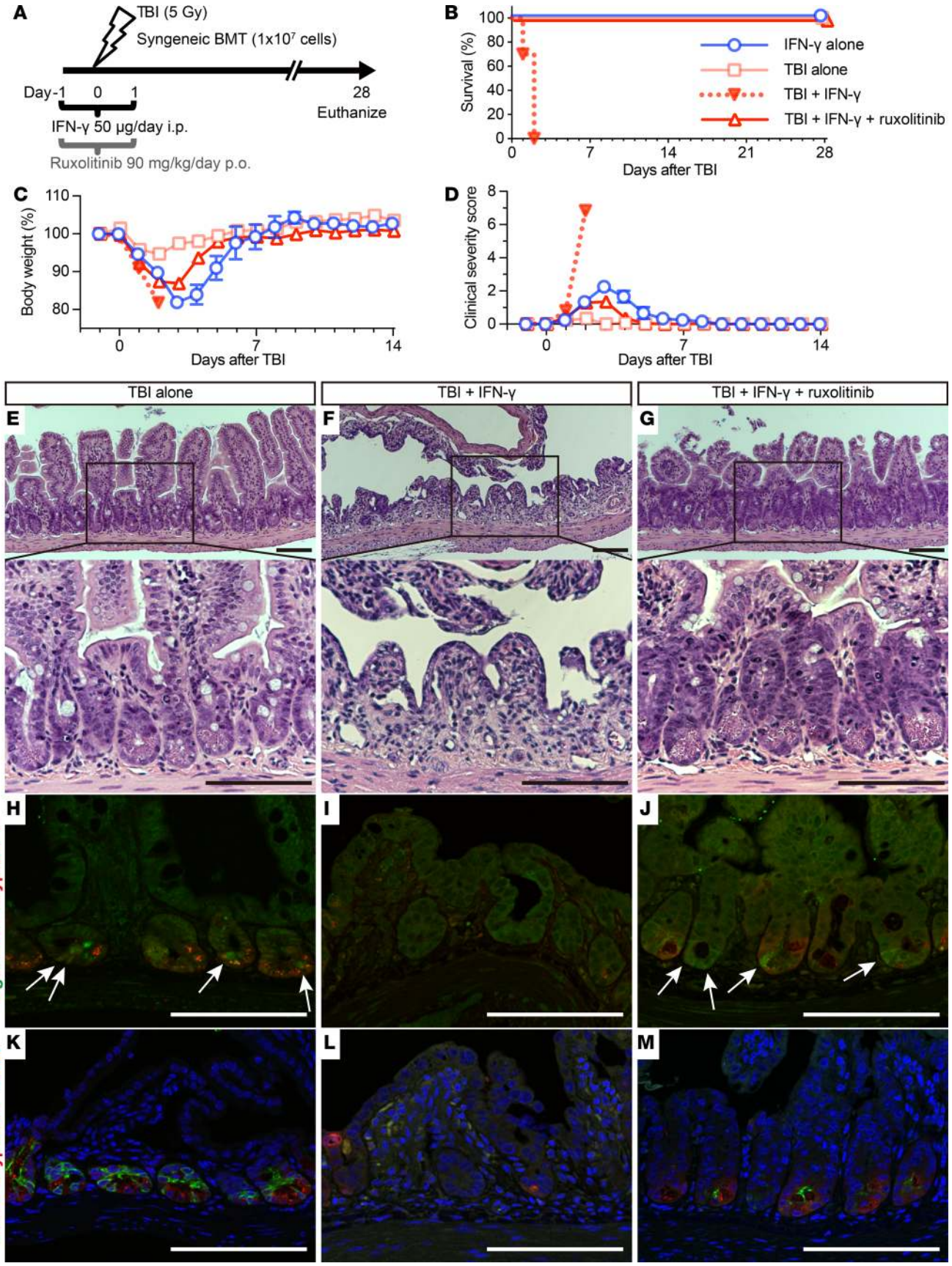
A
TBI (5 Gy)
Syngeneic BMT (1x10⁷ cells)
Day-1
0
1
28
Euthanize
IFN-γ 50 μg/day i.p.
Ruxolitinib 90 mg/kg/day p.o.
B
Survival (%)
Days after TBI
IFN-γ alone
TBI alone
TBI + IFN-γ
TBI + IFN-γ + ruxolitinib
C
Body weight (%)
Days after TBI
D
Clinical severity score
Days after TBI
TBI alone
TBI + IFN-γ
TBI + IFN-γ + ruxolitinib
E
F
G
H
I
J
Lgr5-GFP
Cryptdin-1
K
L
M
Olfm4
Cryptdin-1
DAPI

Figure 11. IFN-γ increases the radiosensitivity of intestinal epithelial tissue. (**A**) Schematic depiction of TBI, and IFN-γ and ruxolitinib administration in mice. After TBI, mice received syngeneic bone marrow transplantation (BMT) to rescue from bone marrow death on day 0. Survival (**B**), body weight as a percentage of initial weight (**C**), and clinical severity scores (**D**) from 2 independent experiments were combined, and data are shown as mean values ± SEM (IFN-γ alone group, n = 6; TBI alone group, n = 6; TBI + IFN-γ group, n = 10; TBI + IFN-γ + ruxolitinib group, n= 10). (**E**–**M**) Histology of mouse ileal sections 48 hours after TBI. H&E staining of ileum sections from mice receiving TBI (**E**), TBI + IFN-γ (**F**), or TBI + IFN-γ + ruxolitinib (**G**). (**H**–**M**) Confocal imaging of *Lgr5-EGFP-ires-creERT2* mouse ileum sections. Immunofluorescence staining of cryptdin-1 (red, **H**-**M**), Lgr5-GFP$^+$ (green, white arrows, **H**-**J**), Olfm4 (green) and DAPI (blue) (**K**-**M**) for mice that received TBI (**H** and **K**), TBI + IFN-γ (**I** and **L**), or TBI + IFN-γ + ruxolitinib (**J** and **M**). The results are representative of 2 separate experiments and illustrate the reduction in crypt numbers and the loss and absence of Paneth cells and rapidly cycling ISCs in ileum of TBI + IFN-γ–treated mice (**F**, **I**, and **L**). Scale bars: 100 μm.

lipopolysaccharide translocation across the damaged gut barrier. Those conditions stimulate donor T cells further and accelerate disease (9), which ruxolitinib ameliorates by increasing regulatory T cell numbers (31) and altering T cell trafficking (22) in GVHD mice. Also, in 2 patients with corticosteroid-refractory intestinal GVHD, ruxolitinib treatment reduced disease severity (31) and resulted in improvement of gut GVHD. We have focused in this report on direct adverse effects on small intestinal epithelial lineages and ISCs mediated by IFN-γ. The efficacy of ruxolitinib in preventing IFN-γ–induced effects and damage both ex vivo and in vivo identifies Paneth cells and the epithelium as potentially new cell targets for this therapeutic agent.

Methods

Mice. Female C57BL/6, B6.1297S7-*Ifngr1*$^{tm1.Agt}$/J, and *Lgr5-EGFP-ires-creERT2* mice were purchased from the Jackson Laboratory or Japan SLC, Hamamatsu.

Enteroid culture. Crypt isolation and enteroid culture were performed as previously described (7). Crypts were isolated from mouse ilea by incubation for 30 minutes at 4°C in PBS containing 2 mM EDTA. A total of 50 crypts were mixed with 10 μl Matrigel Growth Factor Reduced (Corning) and plated in 96-well plates. After the Matrigel polymerized, culture medium (Advanced DMEM/F12 supplemented with 100 U/ml penicillin, 100 μg/ml streptomycin, 10 mM HEPES, 2 mM Glutamax, 1× N2 supplement, 1× B27 supplement [all from Thermo Fisher Scientific], 1 mM *N*-acetylcysteine [Sigma-Aldrich], 50 ng/ml mouse EGF [PeproTech], 100 ng/ml mouse Noggin [PeproTech], and 1 μg/ml human R-spondin 1 [R&D Systems]) was added. Culture media were replaced every 4 days. For passage, enteroids were removed from Matrigel and mechanically dissociated into single-crypt domains, and then transferred to fresh Matrigel. Passage was performed every 1–2 weeks, with a 1:5 split ratio. Every experiment was started on day4 after enteroid passage.

For T cell coculture experiments, CD4$^+$ and CD8$^+$ T cells were isolated with CD4 and CD8a MicroBeads (Miltenyi Biotec) from C57BL/6 mouse splenocytes. T cells or splenocytes were cocultured at a ratio of 50,000 cells per 40–60 enteroids, which were embedded in Matrigel. T cells were activated by addition of Dynabeads Mouse T-Activator CD3/CD28 (Thermo Fisher Scientific) to cultures.

For experiments evaluating the effects of cytokines on enteroids, rmIL-2, rmIL-6, rmIL-17A, rmIFN-γ, rmTNF-α were added to culture wells (BioLegend). In some experiments, enteroids were cultured in the presence of ruxolitinib (SelleckChem).

To evaluate disruption of enteroid integrity, an enteroid damage scoring system was established as follows: normal condition, 1; partial disruption or loss of crypt domains, 2; enteroid dissociation >50%, 3; and complete enteroid dissociation, 4.

Cytokine ELISA assay. Conditioned media were collected from enteroid cultures and stored at −20°C. Cytokine ELISA assays were performed using mouse IL-2, IL-6, IL-17A, IFN-γ, and TNF-α ELISA MAX Deluxe (BioLegend) and performed according to the manufacturer's protocol.

qRT-PCR. Total RNA was extracted using TRIzol Reagent (Thermo Fisher Scientific). cDNA was synthesized using a PrimeScript RT Reagent kit with gDNA Eraser (TaKaRa Bio). Quantitative RT-PCR was performed using a LightCycler 480 Instrument II (Roche) with LightCycler 480 SYBR Green I Master (Roche) and gene-specific primers (Supplemental Table 1). The relative amount of each mRNA was calculated by the cycling threshold (Ct) method as $2^{-\Delta\Delta Ct}$ normalized to *Gapdh* of control samples at the same time point.

Live imaging. For phase contrast microscopy, enteroids were cultured as described above. Images were captured using an Eclipse TE2000-U microscope (Nikon), SPOT RT-KE Camera, and SPOT 5.1 Advanced software (Diagnostic Instruments). For confocal time-lapse analysis, enteroids were exposed to 2 ng/ml IFN-γ with CellEvent caspase-3/7 Green Detection Reagent (Thermo Fisher Scientific) for 18 hours. Live imaging

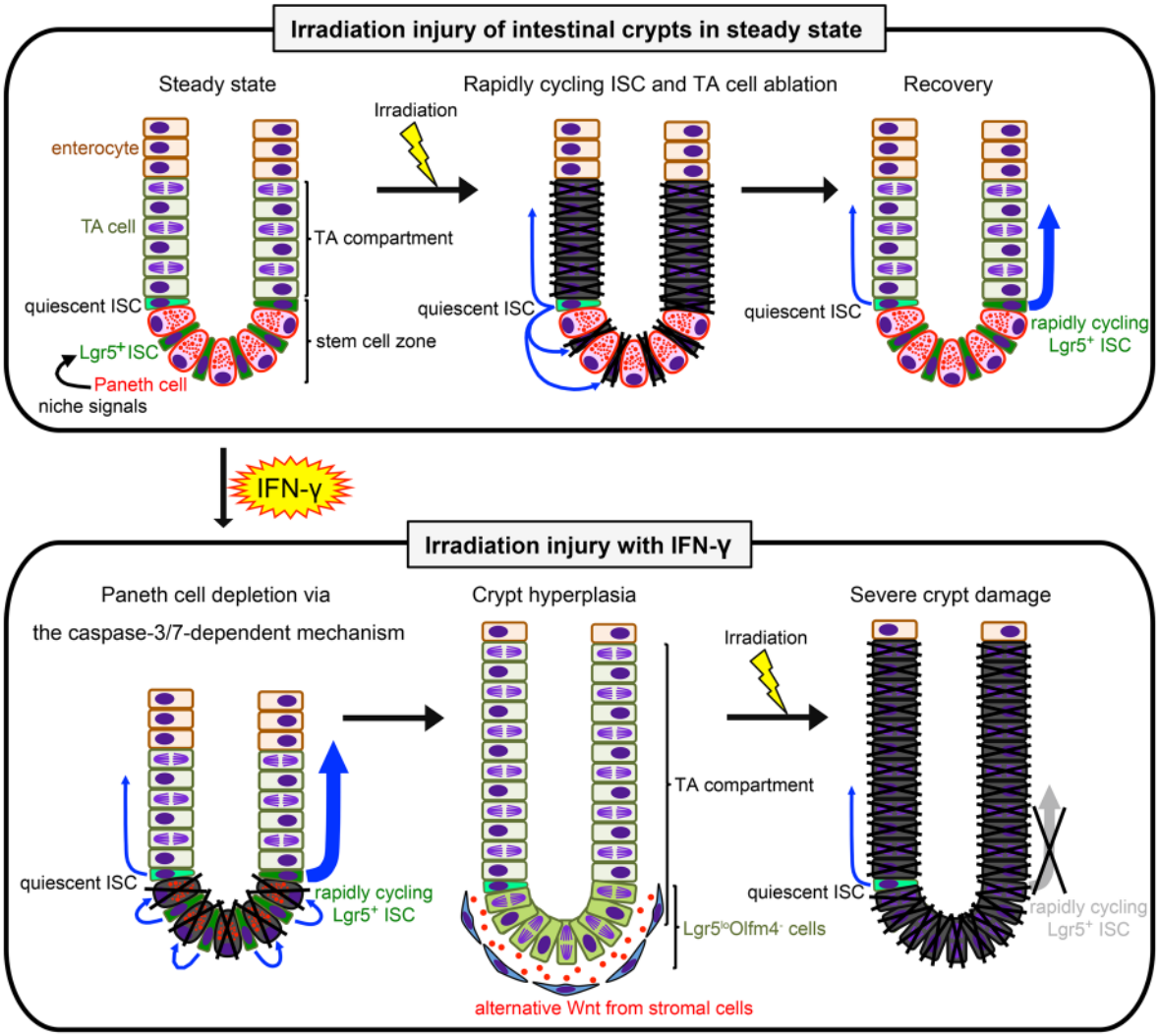

Figure 12. Schematic representation of hypothetical IFN-γ etiology augmenting irradiation injury. Upper images depict the course of crypt recovery from irradiation injury. Rapidly cycling ISCs that converted from quiescent ISCs after irradiation (center image, blue arrows) restore damaged crypts promptly (33, 34). Lower panel shows the hypothetical IFN-γ etiology. In the absence of niche signals previously derived from Paneth cells, Lgr5^{lo}Olfm4^{-} cells, and TA cells become prevalent, and Lgr5^{lo}Olfm4^{-} cells replace positions the base of the crypts that formerly were occupied by the depleted Paneth cells. The increase in Lgr5^{lo}Olfm4^{-} cells relative to Lgr5^{+}Olfm4^{+} ISCs may contribute to crypt hyperplasia. However, in crypts depleted of Paneth cells by IFN-γ exposure, *Bmi1*$^{+}$ quiescent ISCs cannot convert to rapidly cycling ISCs in sufficient numbers to respond to irradiation, resulting in failure to repair and restore epithelial integrity. Blue arrows indicate ISC division.

was acquired by confocal microscopy (A1, Nikon) at 37°C with 5% CO_2. A *Z*-stack was acquired every 10 minutes for 10–16 hours. Reconstruction of images was done using NIS-Element C version 4.40 software.

Histological and immunofluorescence analysis. For pathological analysis, samples of the ileum were fixed in 4% paraformaldehyde, embedded in paraffin, and examined by H&E staining and a spectrum of immunofluorescence reactions. The primary antibodies were chicken anti-GFP (1:500, ab13970, Abcam), rabbit anti-Olfm4 (1:200, D6Y5A, Cell Signaling Technology), rabbit anti–Ki-67 mAb (1:400, D3B5, Cell Signaling Technology), and rat anti-Crp1 mAb (1 μg/ml, clone 77-R63) generated following immunization of rats with synthetic mouse cryptdin-1 (32). The secondary antibodies were Alexa Fluor 488–conjugated anti-chicken IgG (A-11039), Alexa Flour 488–conjugated anti-rabbit IgG (A-11034), and Alexa Fluor 594–conjugated anti-rat IgG (A-11007) purchased from Life Technologies. Immunohistochemistry Application Solutions Kit (Rabbit) (Cell Signaling Technology) was used for IHC staining. DNA was stained by DAPI (Molecular Probes). Pictures from tissue sections were taken at room temperature using a digital camera (DS-Ri2, Nikon) mounted on a microscope (Eclipse TE2000 or A1, Nikon) and NIS-Element Br version 4.40 software. All crypts present within 50 μm of the muscularis

externa were counted per ileum circumference section after staining for cryptdin-1, GFP, and Olfm4 of *Lgr5-EGFP-ires-creERT2* ileum.

Drug administration. Mice were injected i.p. with 50 μg mouse IFN-γ (GenScript) dissolved in 1.5 ml saline or vehicle daily in 3 equal doses every 8-hour interval for 3 days. Ruxolitinib (LC Laboratories) was dissolved in ethanol and mixed with PBS with 0.1% Tween-20. Mice received 30 mg/kg ruxolitinib p.o. in 200 μl vehicle by oral gavage 3 times per day for 3 days. The control group received vehicle alone.

Irradiation and BMT. The mice were given sublethal TBI in a single 5-Gy dose using an X-RAD 320ix instrument (Precision X-Ray) 24 hours after the first administration of IFN-γ or vehicle. Then, mice were injected i.v. with 1×10^7 syngeneic bone marrow cells to rescue from bone marrow death. Mice were maintained under specific pathogen–free conditions and received normal chow and filtered water. Survival, body weight, and severity of clinical manifestations were monitored daily until 28 days after TBI. Clinical severity scores were assessed by the sum of changes in 5 clinical parameters: weight loss, posture, activity, fur texture, and skin integrity (maximum index, 10) as previously described (9).

Small intestinal crypt cell preparation and flow cytometry. For crypt isolation, the villi of *Lgr5-EGFP-ires-CreERT2* mouse small intestine were scraped off using a scalpel blade, and remaining tissues were washed with cold PBS. After incubation with 30 mM EDTA in HBSS for 10 minutes at room temperature, the tissue fragments were shaken vigorously in fresh HBSS to exfoliate crypts. The dissociated crypts were further digested with shaking at 180 rpm in HBSS supplemented with 300 U/ml collagenase (Sigma-Aldrich), 10 μM Y-27632 (Sigma-Aldrich), and 1 mM *N*-acetylcysteine for 5 minutes at 37°C on a horizontal shaker (TAITEC). Crypt cells were then briefly treated with 50 μg/ml DNase I (Roche), filtered with a 40-μm cell strainer (Corning), and washed with DMEM/F12 supplemented with 10 μM Y27632 and 1 mM *N*-acetyl-L-cysteine. 5×10^6 crypt cells were incubated with primary antibodies: Brilliant Violet 421–conjugated rat anti-mouse CD24 mAb (2.5 μg/ml, M1/69, BioLegend) and biotinylated hamster anti–mouse CD119 (Ifngr1) mAb (5 μg/ml, 2E2, BD Biosciences); or stained with matched isotype control IgG: Brilliant Violet 421–conjugated rat IgG Ctrl antibody (2.5 μg/ml, RTK4530, BioLegend) and hamster IgG monoclonal isotype control (5 μg/ml, 299Arm, Abcam) biotinylated with Biotin Labeling kit-NH_2 (Dojindo) for 10 minutes at room temperature. After washing with sorting buffer (2% FBS in PBS), crypt cells were incubated with biotinylated goat anti-hamster IgG Ab (5 μg/ml, Poly4055, BioLegend) for 10 minutes at room temperature, washed with sorting buffer, and subsequently incubated with APC Streptavidin (5 μg/ml, BioLegend) for 10 minutes at 4°C. Cells were washed with sorting buffer, filtered with a 35-μm cell strainer (Corning), and subjected to Paneth cell and $Lgr5^+$ ISC subpopulation analysis using a JSAN cell sorter (Bay Bioscience) and FlowJo software version 10.4.2 (TreeStar Inc.). The sorted Paneth cell subpopulation was incubated with 10 μM Zinpyr-1 (Santa Cruz Biotechnology Inc.) for 10 minutes at 37°C to stain secretory granules and identified as Paneth cells using a confocal microscope (A1, Nikon).

Statistics. Groups were compared using 1-way ANOVA with Dunnett's multiple comparisons test, 1-way ANOVA with Tukey's multiple comparisons test, or 2-tailed unpaired *t* test, as indicated in the figure legends. All tests were performed with GraphPad Prism version 7 software. Statistical significance for comparisons was assigned at $^*P < 0.05$, $^{**}P < 0.01$, $^{***}P < 0.001$, and $^{****}P < 0.0001$.

Study approval. All animal experiments were performed with approval of the Institutional Animal Care and Use Committee of University of Southern California and under the auspices of the Institutional Animal Care and Research Advisory Committee of Hokkaido University.

Author contributions

YE and AJO developed the conceptual framework of the study; YE designed and performed experiments and analyzed data; YE and AJO wrote the manuscript; YY, KN, RS, and ST conducted experiments; KN, TA, DH, and TT supervised experiments. MES analyzed data and edited the manuscript.

Acknowledgments

This study was supported by NIH grants R21AI105057 (AJO) and R01AI22931 (MES); a fellowship (2013-2014) from the Uehara Memorial Foundation, Tokyo, Japan (YE); Grants-in-Aid for Scientific Research from the Japan Society for the Promotion of Science 26462831 (KN) and 17H04206 (TT); the Ministry of Education, Culture, Sports, Science, and Technology of Japan (TA); and the Center of Innovation Program from the Japan Science and Technology Agency (KN). This work was also supported in part by USC Norris Cancer Center Support Grant P30CA014089 from the National Cancer Institute.

Address correspondence to: Yoshihiro Eriguchi, Department of Pathology and Laboratory Medicine, Keck School of Medicine, University of Southern California, USC Norris Comprehensive Cancer Center, NRT 7514, 1450 Biggy Street, Los Angeles, California 90089-9601, USA. Phone: 323.442.7955; Email: eriguchi@usc.edu.

1. Clevers HC, Bevins CL. Paneth cells: maestros of the small intestinal crypts. *Annu Rev Physiol*. 2013;75:289–311.
2. Ayabe T, Satchell DP, Wilson CL, Parks WC, Selsted ME, Ouellette AJ. Secretion of microbicidal alpha-defensins by intestinal Paneth cells in response to bacteria. *Nat Immunol*. 2000;1(2):113–118.
3. Salzman NH, Ghosh D, Huttner KM, Paterson Y, Bevins CL. Protection against enteric salmonellosis in transgenic mice expressing a human intestinal defensin. *Nature*. 2003;422(6931):522–526.
4. Salzman NH, et al. Enteric defensins are essential regulators of intestinal microbial ecology. *Nat Immunol*. 2010;11(1):76–83.
5. Masuda K, Sakai N, Nakamura K, Yoshioka S, Ayabe T. Bactericidal activity of mouse α-defensin cryptdin-4 predominantly affects noncommensal bacteria. *J Innate Immun*. 2011;3(3):315–326.
6. Salzman NH, Bevins CL. Dysbiosis — a consequence of Paneth cell dysfunction. *Semin Immunol*. 2013;25(5):334–341.
7. Sato T, et al. Paneth cells constitute the niche for Lgr5 stem cells in intestinal crypts. *Nature*. 2011;469(7330):415–418.
8. Yilmaz ÖH, et al. mTORC1 in the Paneth cell niche couples intestinal stem-cell function to calorie intake. *Nature*. 2012;486(7404):490–495.
9. Eriguchi Y, et al. Graft-versus-host disease disrupts intestinal microbial ecology by inhibiting Paneth cell production of α-defensins. *Blood*. 2012;120(1):223–231.
10. Eriguchi Y, et al. Decreased secretion of Paneth cell α-defensins in graft-versus-host disease. *Transpl Infect Dis*. 2015;17(5):702–706.
11. Levine JE, et al. Low Paneth cell numbers at onset of gastrointestinal graft-versus-host disease identify patients at high risk for nonrelapse mortality. *Blood*. 2013;122(8):1505–1509.
12. Raetz M, et al. Parasite-induced TH1 cells and intestinal dysbiosis cooperate in IFN-γ-dependent elimination of Paneth cells. *Nat Immunol*. 2013;14(2):136–142.
13. Burger E, et al. Loss of Paneth cell autophagy causes acute susceptibility to Toxoplasma gondii-mediated inflammation. *Cell Host Microbe*. 2018;23(2):177–190.e4.
14. Al Khalidi H, Kandel G, Streutker CJ. Enteropathy with loss of enteroendocrine and paneth cells in a patient with immune dysregulation: a case of adult autoimmune enteropathy. *Hum Pathol*. 2006;37(3):373–376.
15. Singhi AD, Goyal A, Davison JM, Regueiro MD, Roche RL, Ranganathan S. Pediatric autoimmune enteropathy: an entity frequently associated with immunodeficiency disorders. *Mod Pathol*. 2014;27(4):543–553.
16. Masia R, Peyton S, Lauwers GY, Brown I. Gastrointestinal biopsy findings of autoimmune enteropathy: a review of 25 cases. *Am J Surg Pathol*. 2014;38(10):1319–1329.
17. Greenson JK. The biopsy pathology of non-coeliac enteropathy. *Histopathology*. 2015;66(1):29–36.
18. Farin HF, et al. Paneth cell extrusion and release of antimicrobial products is directly controlled by immune cell-derived IFN-γ. *J Exp Med*. 2014;211(7):1393–1405.
19. Sato T, et al. Single Lgr5 stem cells build crypt-villus structures in vitro without a mesenchymal niche. *Nature*. 2009;459(7244):262–265.
20. Farin HF, Van Es JH, Clevers H. Redundant sources of Wnt regulate intestinal stem cells and promote formation of Paneth cells. *Gastroenterology*. 2012;143(6):1518–1529.e7.
21. VanDussen KL, et al. Notch signaling modulates proliferation and differentiation of intestinal crypt base columnar stem cells. *Development*. 2012;139(3):488–497.
22. Choi J, et al. IFNγR signaling mediates alloreactive T-cell trafficking and GVHD. *Blood*. 2012;120(19):4093–4103.
23. Serra S, Jani PA. An approach to duodenal biopsies. *J Clin Pathol*. 2006;59(11):1133–1150.
24. Durand A, et al. Functional intestinal stem cells after Paneth cell ablation induced by the loss of transcription factor Math1 (Atoh1). *Proc Natl Acad Sci USA*. 2012;109(23):8965–8970.
25. Kim TH, Escudero S, Shivdasani RA. Intact function of Lgr5 receptor-expressing intestinal stem cells in the absence of Paneth cells. *Proc Natl Acad Sci USA*. 2012;109(10):3932–3937.
26. Kabiri Z, et al. Stroma provides an intestinal stem cell niche in the absence of epithelial Wnts. *Development*. 2014;141(11):2206–2215.
27. Shoshkes-Carmel M, et al. Subepithelial telocytes are an important source of Wnts that supports intestinal crypts. *Nature*. 2018;557(7704):242–246.
28. Samuelson LC. Debate over the identity of an intestinal niche-cell population settled. *Nature*. 2018;558(7710):380–381.
29. Guy-Grand D, DiSanto JP, Henchoz P, Malassis-Séris M, Vassalli P. Small bowel enteropathy: role of intraepithelial lymphocytes and of cytokines (IL-12, IFN-gamma, TNF) in the induction of epithelial cell death and renewal. *Eur J Immunol*. 1998;28(2):730–744.
30. Cheng H, Merzel J, Leblond CP. Renewal of Paneth cells in the small intestine of the mouse. *Am J Anat*. 1969;126(4):507–525.
31. Spoerl S, et al. Activity of therapeutic JAK 1/2 blockade in graft-versus-host disease. *Blood*. 2014;123(24):3832–3842.
32. Hayase E, et al. R-Spondin1 expands Paneth cells and prevents dysbiosis induced by graft-versus-host disease. *J Exp Med*. 2017;214(12):3507–3518.
33. Tian H, et al. A reserve stem cell population in small intestine renders Lgr5-positive cells dispensable. *Nature*. 2011;478(7368):255–259.
34. Metcalfe C, Kljavin NM, Ybarra R, de Sauvage FJ. Lgr5+ stem cells are indispensable for radiation-induced intestinal regeneration. *Cell Stem Cell*. 2014;14(2):149–159.